

TTL cooling and drying during the January 2013 stratospheric sudden warming

Stephanie Evan,^{a*} K. H. Rosenlof,^b Troy Thornberry,^{b,c} Andrew Rollins^{b,c} and Sergey Khaykin^d

^aLaboratoire de l'Atmosphère et des Cyclones, Saint-Denis, France

^bChemical Sciences Division, Earth System Research Laboratory, NOAA, Boulder, CO, USA

^cCooperative Institute for Research in Environmental Sciences, University of Colorado, Boulder, USA

^dLaboratoire Atmosphères Milieux Observations Spatiales, Paris, France

*Correspondence to: S. Evan, UMR8105 LACy, Université de la Réunion, 15 Avenue René Cassin, CS 92003 Saint-Denis Cedex 9, France. E-mail: stephanie.evan@univ-reunion.fr

Extremely low water vapour concentrations (as low as 1.5 ppmv) in the tropical tropopause layer (TTL) were observed by *in situ* measurements during the Airborne Tropical TRopopause Experiment (ATTREX) winter 2013 deployment in February 2013. The January 2013 tropical (15°N – 15°S) mean value of Microwave Limb Sounder (MLS) water vapour satellite data at 82 hPa (2.3 ppmv) was one of the lowest during the instrument record (2004–2013). The relationship between a cooling of the tropical tropopause, a sudden stratospheric warming (SSW) event and convective activity in the western Pacific is investigated using satellite data and reanalysis meteorological products to elucidate the likely origin of those extremely low water vapour concentrations.

A major midwinter SSW developed on 6 January 2013. Stratospheric polar temperatures increased by $\sim 30\text{ K}$ in a matter of days and temperatures in the tropical upper troposphere and lower stratosphere (UTLS) dropped at the same time. As a result of the easterly shear phase of the Quasi-Biennial Oscillation and the SSW, the tropical tropopause in January 2013 was anomalously cold (zonal mean of 187 K) and elevated (85 hPa). The tropical cold point tropopause (CPT) temperature and water vapour concentration at 82 hPa decreased by about 2 K and 1.5 ppmv respectively within the first 15 days of January; the water vapour change was likely a result of dehydration associated with the rapid cooling of the tropical CPT during that period.

Key Words: TTL; water vapour; sudden stratospheric warming

Received 1 October 2014; Revised 26 April 2015; Accepted 14 May 2015; Published online in Wiley Online Library 11 August 2015

1. Introduction

Anomalies in water vapour on the order of 0.5 ppmv are significant from a radiative standpoint; Solomon *et al.* (2010) concluded that a similarly sized drop at the end of 2000 may have slowed the rate of increase in global surface temperatures by 25% as compared to what would have been expected from increases in well-mixed greenhouse gases alone over the period 2000–2009. The coldest temperatures encountered at the tropical tropopause (here we use the Cold Point Tropopause, CPT) control the amount of water entering the stratosphere (Brewer, 1949). The CPT temperature depends on overshooting convection (e.g. Kuang and Bretherton, 2004), the large-scale stratospheric circulation (e.g. Gettelman and Birner, 2007), the Quasi-Biennial Oscillation (QBO) (e.g. Plumb and Bell, 1982) and radiative effects of cirrus clouds (e.g. Evan *et al.*, 2013). Several studies have also showed that Kelvin waves can modulate the CPT temperature and height (e.g. Shimizu and Tsuda, 2000; Dima and Wallace, 2007).

The focus of this article is an event during Northern Hemisphere (NH) winter 2013 where multiple observations showed extremely low water vapour concentrations in the tropical tropopause layer (TTL). During this time, the Airborne Tropical TRopopause Experiment (ATTREX) was making high-altitude aircraft measurements, and there were coordinated balloon measurements as well as coincident satellite measurements. For a particular flight day, 26 February 2013, measurements from balloon and aircraft indicated concentrations as low as 1.5 ppmv in the TTL. Those measurements were in agreement with low Microwave Limb Sounder (MLS) satellite values of water vapour (~ 2 ppmv) observed at 82 hPa in the eastern Pacific around 26 February. This is much lower than the normal NH wintertime values; the seasonal variation of entry of water vapour mixing ratios ranges from ~ 2.5 ppmv during January–February to ~ 4.5 ppmv during September–October (Fueglistaler *et al.*, 2005).

The MLS data showed these extremely dry concentrations existing as early as January and covering a large area in the Tropics. The January zonally averaged tropical monthly mean value of MLS

water vapour satellite data at 82 hPa (2.3 ppmv) was one of the lowest during the MLS record (2004–2013); the seasonal mean anomaly for December–January–February 2012/2013 at 82 hPa was -0.53 ppmv. Monthly average values this low only occurred at one other time in the MLS record; this happened during boreal winter 2006. Both events were associated with an easterly shear phase of the QBO, a major sudden stratospheric warming (SSW) and strong convection over the western Pacific.

An SSW corresponds to a rapid temperature increase (>30 – 40 K) in the polar vortex over a few days in the high-latitude stratosphere during the winter. If net zonal-mean zonal winds become easterly north of 60°N at 10 hPa or below, coupled with a polar temperature increase, then the warming is considered to be a major warming (McInturff, 1978). SSWs are preceded by an increase in wave activity from the troposphere that propagate upward and ultimately dissipate in the stratosphere (Matsuno, 1971). These waves break at critical levels where the background wind speed is equal to the wave phase speed. They cause a convergence of wave fluxes, which drives a poleward meridional circulation in the extratropical stratosphere, with upward motion in the Tropics and downward motion in high latitudes (Holton *et al.*, 1995). The change in the meridional circulation induces adiabatic cooling in the equatorial lower stratosphere while warming the polar stratosphere.

Gomez-Escolar *et al.* (2014) showed that, around 50–70 hPa in the tropical stratosphere, an enhanced cooling from an SSW-related stratospheric perturbation occurs preferentially during QBO easterly shear phase. They explain it by anomalous subtropical wave breaking related to changes in the zero-wind line position with the QBO phase. The QBO winds influence the propagation of extratropical planetary waves. Planetary waves are unable to propagate through easterly winds (Charney and Drazin, 1961), and so when the QBO is in its easterly phase, waves are confined more strongly to the Northern Hemisphere extratropical latitudes and wave activity in these regions is stronger than when the QBO is in its westerly phase (Holton and Tan, 1980). In the easterly phase of the QBO the zero-wind line extends further poleward, and consequently there is enhanced subtropical wave dissipation in the lower stratosphere. This results in increased upwelling and cooling in the tropical lower stratosphere.

Previous studies have investigated the impact of SSWs on the TTL (Kodera, 2006; Eguchi and Kodera, 2010; Kodera *et al.*, 2011; Yoshida and Yamazaki, 2011; Eguchi *et al.*, 2015). These studies indicated that strengthening of the tropical upwelling during the SSW event leads to a cooling of the tropical lower stratosphere and upper troposphere. Based on Global Circulation Model (GCM) experiments, Thuburn and Craig (2000) showed that the stratospheric meridional circulation could influence the tropical tropopause. Their GCM experiments with an enhanced Brewer–Dobson circulation in the stratosphere produced a cooler and higher tropopause in the Tropics and warming at high latitudes, a situation similar to the scenario of the January 2013 SSW.

In this article, we postulate that the extremely low water vapour concentration measured in the TTL was a consequence of the interactions between the SSW event in January 2013, the QBO and the Madden–Julian Oscillation (MJO). Reanalysis data from the ECMWF Reanalysis Interim (ERA-Interim) are used solely to estimate changes in the stratospheric circulation associated with the SSW. The article is organized as follows. Observational datasets used (both *in situ* and satellite) are described in section 2. Results are presented in section 3, followed by a summary in section 4.

2. Data

In situ measurements of water vapour were taken from February 2013 through to early March 2013 as part of the second deployment of ATTREX, a multi-year airborne science

campaign designed to better understand processes controlling the TTL region. The campaign used the National Aeronautics and Space Administration (NASA) long-range high-altitude Global Hawk (GH) unmanned aircraft system to study water vapour distributions and cirrus formation in the TTL. The ATTREX payload included multiple instruments to measure cloud properties, trace gases, temperature and water vapour. During the second deployment of ATTREX, six flights were conducted from NASA Dryden Flight Research Center in California into the deep Tropics.

Included on the payload were two water vapour instruments. We include plots with data from the National Oceanic and Atmospheric Administration (NOAA) Water Vapor Instrument, a two-channel, closed-path, tunable diode laser absorption spectrometer designed for the measurement of water vapour and enhanced total water (vapour + inertially enhanced condensed-phase) in the upper troposphere/lower stratosphere (Thornberry *et al.*, 2014). We also use data from the NOAA Frost Point Hygrometer (FPH) balloon profile. This is a compact, lightweight, balloon-borne instrument in which a frost-point temperature is deduced through control of a thin layer of ice on a temperature-controlled mirror (Mastenbrook and Oltmans, 1983; Hurst *et al.*, 2014). The Hilo (19.7°N , 155.1°W) launch on 26 February 2013 was done in coordination with the ATTREX flights. It should be noted that Hilo is not located in the deep Tropics but the Hilo NOAA FPH water vapour data are used for comparison with the aircraft measurements in the tropical eastern Pacific.

Aura Microwave Limb Sounder (MLS) v3.3 water vapour data were included to compare with the *in situ* measurements and to evaluate the spatial extent of the dry air mass sampled during ATTREX. We examine water vapour at 82 hPa, which corresponds to the native MLS pressure level closest to the mean cold point tropopause pressure for the period of consideration.

To study the variations in temperature within the TTL and at the CPT, we used Global Positioning System (GPS) radio occultation temperature profiles derived from the Constellation Observing System for Meteorology, Ionosphere and Climate (COSMIC) satellite mission (Anthes *et al.*, 2008, <http://cosmic-io.cosmic.ucar.edu/cdaac/products.html>). Temperature profiles are analysed for the time period spanning December 2012 to February 2013. About 2000 soundings are available per day, spread relatively evenly over the globe. On average, around 500 temperature profiles per day are obtained for the tropical region (30°S – 30°N). COSMIC temperature profiles extend from the surface to 40 km. The profiles are retrieved on a 100 m vertical resolution, although the actual resolution is a function of height and is about 1 km in the TTL (Kursinski *et al.*, 1997). The cold-point tropopause temperature corresponds to the minimum temperature in the COSMIC 100 m vertical resolution profile. The cold-point tropopause altitude is the height of the minimum temperature.

To characterize the stratospheric circulation, we calculated Eliassen–Palm (EP) fluxes (Andrews *et al.*, 1987, p. 128). To do this, we used 6-hourly wind velocity and temperature data from the ERA-Interim reanalysis. ERA-Interim is a global reanalysis describing the state of the atmosphere and land from 1979 to present (Dee *et al.*, 2011). The data have been obtained from the National Center for Atmospheric Research (NCAR) on a 512×256 regular Gaussian grid with resolution of $\sim 0.7^\circ \times 0.7^\circ$. The data are available four times per day on 60 model levels with a top at 0.1 hPa. The vertical resolution in the TTL region is ~ 1.1 km. In the tropical stratosphere between 100 and 1 hPa, the model levels are located at 1.1, 1.6, 2.1, 2.7, 3.4, 4.2, 5.2, 6.4, 8.0, 9.9, 12.3, 15.2, 18.8, 23.3, 28.9, 35.8, 44.3, 54.6, 66.6, 80.4 and 95.7 hPa.

Tropical convection was analysed using the NOAA Outgoing Longwave Radiation (OLR) data (Liebmann and Smith, 1996). Using these data, we identify deep convection during the same time period as COSMIC data.

3. Results

3.1. Water vapour concentrations

During the fifth flight (26–27 February) of the ATTREX deployment, aircraft observations showed low values of water vapour (~ 2 ppmv) in the eastern Pacific. Figure 1 shows three water vapour mixing-ratio profiles taken near Hawaii on February 26. The black line is a NOAA Frost Point Hygrometer balloon profile launched from Hilo (Hawaii) on 26 February 2013, several hours before two Global Hawk profiles from the NOAA Water Vapor Instrument flying during ATTREX. The balloon data plotted on Figure 1 correspond to 250 m averages and the aircraft measurements are every 1 s of flight. The aircraft profiles were designed to intercept air parcels between 100 and 80 hPa sampled by the balloon launched several hours earlier. There are layers of almost constant water vapour in the aircraft measurements that may reflect vertical mixing or simply a uniform temperature history throughout the layers; however we do not have sufficient data to confirm that. Minimum values of approximately 1.5 ppmv from both the aircraft and balloon match very well. This is in agreement with low MLS water vapour (~ 2 ppmv) observed at 82 hPa in the eastern Pacific around 26 February. We study this particular case because we do have correlative measurements from aircraft, balloon and satellite that show that the extremely low values shown in the satellite profiles in Figure 1 are realistic. Additionally, it coincides with very low values of stratospheric water vapour as indicated by satellite measurements.

Figure 2 shows the MLS satellite water vapour time series at 82 hPa from August 2004 to December 2013. This is a zonally (15°S – 15°N) and monthly averaged time series representative of the average stratospheric entry value of water vapour. We also derived time series of CPT temperature from COSMIC measurements for the same period as MLS. The CPT temperature data on Figure 2 also correspond to zonally (15°S – 15°N) and monthly averaged values. Note that the COSMIC mission started in April 2006 so we use GPS data from Challenging Mini-satellite Payload (CHAMP) to compute the CPT temperatures prior to April 2006. CHAMP and COSMIC give very similar zonally and monthly mean CPT temperatures for the period of the two missions overlapped from April 2006 to September 2008 (not shown). Stratospheric water vapour values at 82 hPa are highly correlated with CPT temperatures. The minima in MLS water vapour time series at 82 hPa occur in February, a month after the minima in CPT temperatures in January. The lag between CPT temperature and 82 hPa water vapour is largely

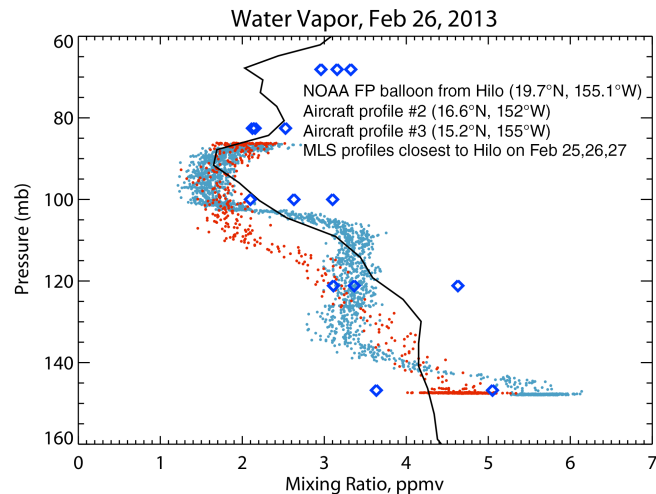


Figure 1. Water vapour profiles. The black line is a NOAA Frost Point Hygrometer balloon profile launched from Hilo (Hawaii) on 26 February 2013, several hours before two Global Hawk profiles from the NOAA Water Vapor Instrument flying during ATTREX (cyan and red dots). The MLS measurements for the profiles nearest Hawaii on 25, 26 and 27 February are shown as blue diamonds.

a consequence of the vertical distance between the CPT and the 82 hPa level. It is well known that tropical CPT temperatures are a controlling factor in setting the entry value of stratospheric water vapour so that the driest values in the MLS water vapour time series follow after the time of the coldest values in the CPT temperature. The year 2012 had the coldest November–December CPT temperatures on the GPS record. The mean CPT temperature for November–December 2012 is 189.5 K, thus an anomaly of -0.8 K compared to the November–December mean CPT over the GPS record (190.3 K). This is consistent with Zhou *et al.*'s (2001) and Yuan *et al.*'s (2014) results, that CPT temperatures are cooler during the easterly shear phase of the QBO. Yuan *et al.* (2014) use 50 years of radiosonde data from ten near-equatorial stations, distributed along the Equator, and show that CPT temperatures during QBO easterly shear conditions are colder than during westerly shear conditions by ~ 0.8 K (cf. Tab. 4 of Yuan *et al.* (2014)).

During the MLS record, the lowest monthly average values occurred during boreal winters 2005/2006 and 2012/2013, with minima of 2.2 and 2.3 ppmv respectively. These two boreal winters had easterly QBO shear, a major SSW in January, and were the coldest in the COSMIC record (CPT temperature of 188.4 and 188.5 K respectively). The winters 2007/2008 and 2009/2010 also had easterly QBO shear, and were cold and relatively dry (189.0 and 189.2 K; 2.5 and 2.7 ppmv). However, they did not experience January SSWs. In this study we will compare the QBO easterly years with January SSWs to 2008 and 2010, without a January SSW.

Both 2006 and 2013 had major SSWs in January (on 21 and 6 January respectively) while 2008 and 2010 had an SSW in February (on 22 and 9 February respectively). To contrast these four years, Figure 3 shows the annual progression of MLS water vapour at 82 hPa for June 2005–2006, June 2007–2008, June 2009–2010 and June 2012–2013. The dry water vapour anomalies were -0.5 ppmv at 82 hPa in February 2006 and 2013. They correspond to differences from the 2004–2013 February mean. These are the largest anomalies seen over the past decade. In contrast to February 2006 and 2013, the dry water vapour anomalies in February 2008 and 2010 are only -0.2 and -0.1 ppmv respectively despite rather cold CPT temperatures in January 2008 and 2010. The impact of SSW, the phase of QBO and convection on the cold and dry values observed for these four years will be discussed in section 4.

3.2. Dynamics of the stratosphere and TTL

A major SSW occurred on 6 January 2013. At this time, the zonal-mean zonal winds at 10 hPa and 60°N switched from westerly to easterly (Figure 4(c)). The January 2013 SSW has easterlies extending down to ~ 40 hPa and westerlies reappeared at all levels by ~ 25 January. 10 hPa polar temperatures (60 – 90°N) rose from 207 K on 26 December to over 234 K on 8 January (Figure 4(a)). At the same time, the 10 hPa temperature averaged over the Tropics (15°S – 15°N) shows a rapid decrease. This is coincident with an increased mean meridional circulation associated with the SSW. It can also be seen from Figure 4(b) (blue line) that there is a 2 K drop in CPT temperature in the first two weeks of November 2012. Note that a drop of 1 K in CPT temperature from November to December is expected as part of the annual cycle in CPT temperature (cf. Figure 2).

We used the ERA-Interim 6-hourly temperature data to compute the zonal mean temperature tendency for October–December 2012. During October 2012, the temperature tendency shows a broad region of tropical cooling (-0.03 K day^{-1}) between the tropopause and ~ 40 hPa as well as a region of warming in the subtropics between the tropopause and ~ 50 hPa (not shown). This pattern is likely a signature of the shallow branch of the Brewer–Dobson circulation, located in the lowermost stratosphere, with upwelling in the Tropics and downwelling in the subtropics and middle latitudes (Birner and Bönisch, 2011). In November 2012, the magnitude of the

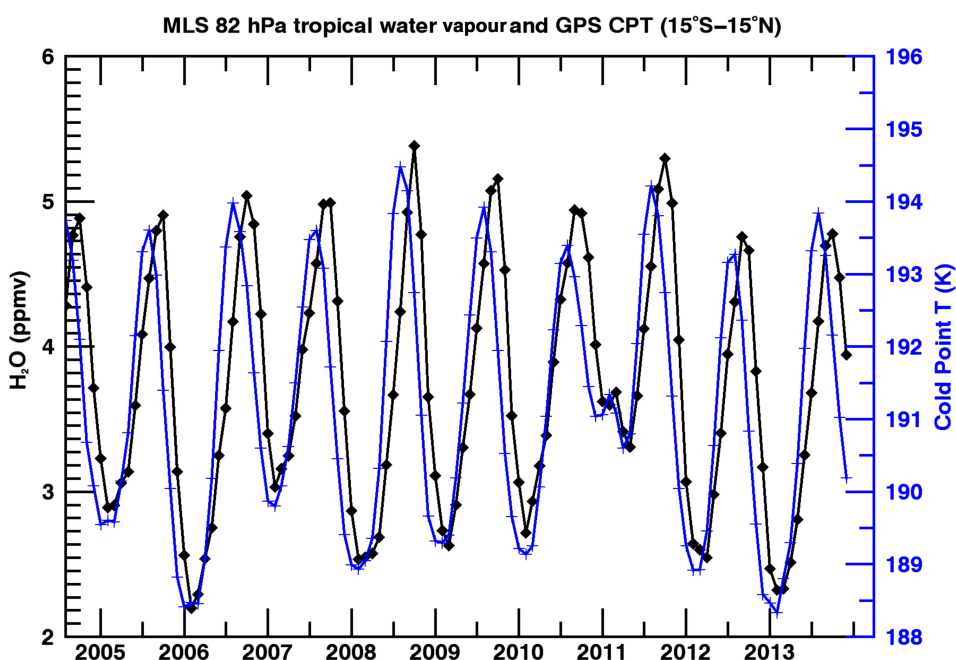


Figure 2. Time series of monthly mean MLS water vapour at 82 hPa (black diamonds) and monthly mean GPS CPT temperature (blue crosses) averaged over 15°S – 15°N .

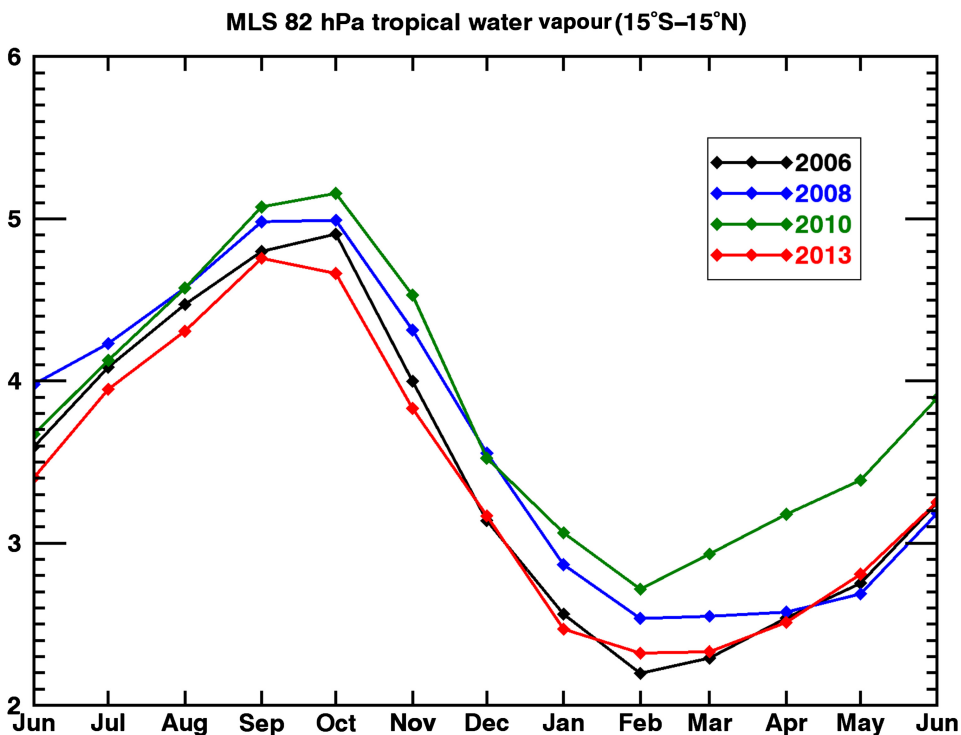


Figure 3. Time series of monthly mean MLS water vapour (ppmv) at 82 hPa averaged over 15°S – 15°N for 2006 (black), 2008 (blue), 2010 (green) and 2013 (red).

cooling/warming increases and this indicates a strengthening of the shallow branch. This is likely related to more subtropical wave driving in the lower stratosphere.

From the end of December to 26 January, the CPT temperature averaged over the Tropics (15°S – 15°N) decreased by $\sim 2.5\text{ K}$ and the CPT altitude increased by $\sim 400\text{ m}$ (green line on Figure 4(b)). The CPT temperature drop is coherent with adiabatic cooling produced by an increase in tropical upwelling. In addition, there was an easterly shear phase of the QBO during winter 2012/2013 (not shown). In periods with descending easterly QBO shear, there is anomalous equatorward motion at low levels and relative upwelling at the Equator (Fig. 1 of Plumb and Bell, 1982). The compensating ascent in the Tropics induces a colder and higher tropopause. Thus additional cooling and lifting of the tropopause is observed in January 2013 because of the easterly shear phase of the QBO. In the Tropics, the temperature change

at 10 hPa is more rapid than the CPT cooling. This suggests that different mechanisms are operating to modify the mean circulation in the stratosphere and tropical UTLS. Gomez-Escalor *et al.* (2014) proposed a mechanism for tropical stratospheric cooling associated with an SSW occurrence (Fig. 8 of Gomez-Escalor *et al.*, 2014). The cooling in the upper tropical stratosphere occurs almost simultaneously with the polar cap warming and is associated with a strengthening of the deep branch of the Brewer–Dobson circulation that connects the tropical and polar regions. They further suggest that the temperature decrease in the lower tropical stratosphere during the easterly phase of the QBO and an SSW is due to large EP flux divergence in the subtropics below 30 hPa, in agreement with the zero-wind line position during an easterly QBO. As a result there is an acceleration of the shallow branch of the Brewer–Dobson circulation and enhanced cooling in the tropical lower stratosphere.

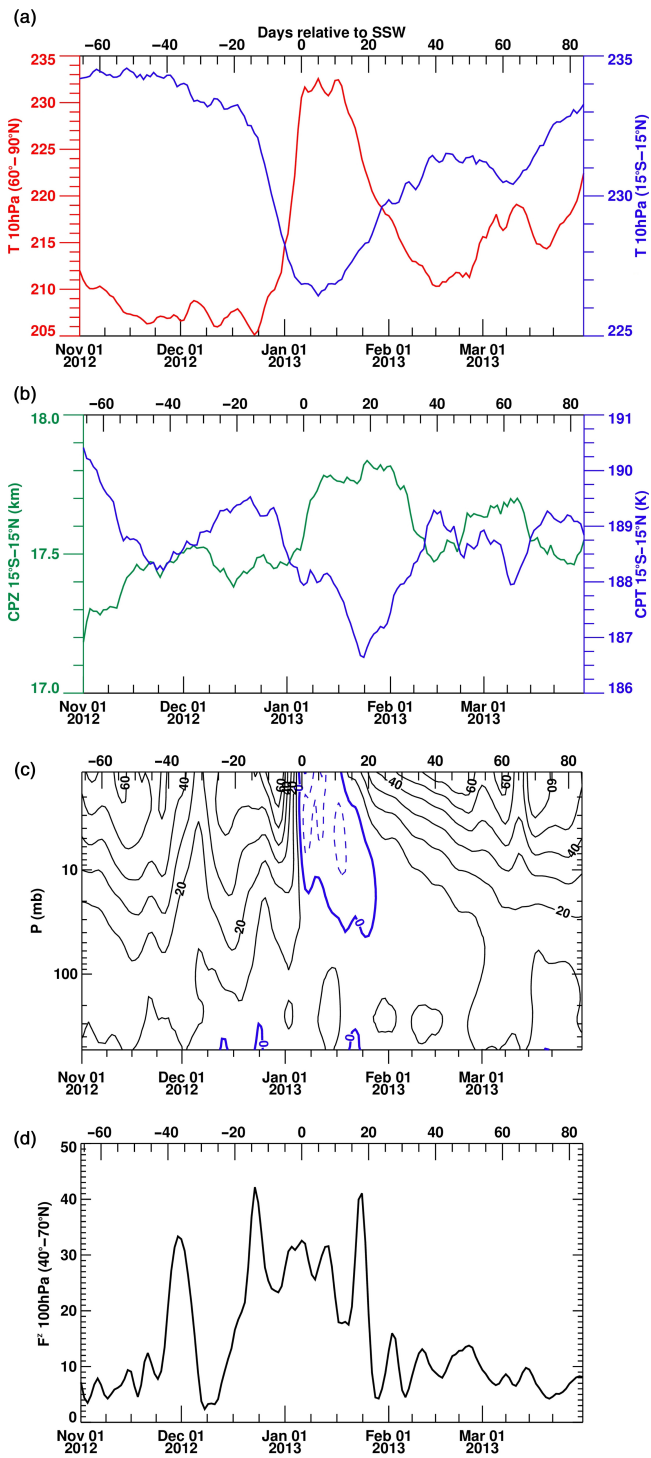


Figure 4. (a) Time series of COSMIC 10 hPa temperatures averaged over 60°–90°N (red line) and 15°S–15°N (blue line). (b) Time series of CPT temperature (blue line) and height (CPZ, green line) averaged over 15°S–15°N. (c) Time–altitude section of zonal-mean zonal wind at 60°N. (d) Time series of the vertical component of EP Flux (10^4 kg s^{-2}) at 100 hPa averaged over 40°–70°N.

To examine the large-scale dynamics, we look at the time series of the vertical component of EP flux F^z at 100 hPa for the boreal winter 2012–2013 (Figure 4(d)). F^z is averaged over the Northern Hemisphere extratropics (40°–70°N) and is used to diagnose the planetary wave activity entering the stratosphere at these latitudes. Three episodes of wave activity emanating from the troposphere occurred in December and early January. Each of these wave events lasted about a week. A first burst of wave activity began in late November and lasted until early December. It was followed by a second burst in mid-December that peaked on 24 December, and shortly after that a third burst of wave activity began on 29 December 2012 and peaked on 6 January

2013. Zonal mean wind at 60°N experiences periods of episodic wind deceleration that occur with a lag of several days behind the enhancement of upward wave propagation from the troposphere observed on Figure 4(d).

Figure 5 shows daily time series of TTL upwelling averaged over 15°S–15°N and between 96 and 67 hPa from November 2012 to March 2013. We use the vertical range 96 to 67 hPa to define TTL upwelling to avoid the tropospheric Hadley cell influence. The years 2006, 2008 and 2010 are also shown for comparison. The upwelling was computed from the residual mass stream function that is defined as:

$$\Psi^* = \Psi - \frac{a}{g} \cos \varphi \frac{\overline{v' \theta'}}{\partial_p \overline{\theta}}, \quad (1)$$

where $\Psi = \frac{a}{g} \cos \varphi \int_0^P \bar{v} dp$ is the stream function in pressure coordinates, over-bars denote zonal averages, v' and θ' are deviations from zonal averages and all other symbols are defined by Andrews *et al.* (1987). The procedure for computing Ψ and Ψ^* follows Juckes (2001) and Birner and Bönisch (2011). The residual vertical velocity is then $\bar{w}^* = \frac{1}{\rho_0 a \cos \varphi} \frac{\partial \Psi^*}{\partial \varphi}$ (cf. Equation 6 of Rosenlof (1995)). Daily mean stream function and residual vertical velocity are obtained using the 6-hourly data. The mean TTL upwelling is 0.6, 0.35, 0.48 and 0.7 mm s⁻¹ for January 2006, 2008, 2010 and 2013 respectively. The stronger TTL upwelling during January 2013 corresponds with the cooler CPT observed during that period. TTL upwelling was also strong (0.6 mm s⁻¹) in November 2012 and could explain some of the rapid cooling at the beginning of November.

When comparing the mean CPT temperatures for January 2006, 2008, 2010 and 2013 there are several aspects to consider: the mean value of TTL upwelling, the phase of the QBO and the deep convection in the Tropics. The easterly QBO shear, measured as the difference between the zonal-mean zonal wind at 50 and 100 hPa, was similar for boreal winters 2006, 2008 and 2013 (-10 m s^{-1}) and somewhat weaker in boreal winter 2010 (-6 m s^{-1}). This would result in similar cold temperature anomalies in the lower stratosphere. The MJO was active during the four boreal winters with comparable intensity. This will be discussed in more detail in subsection 3.3. However January 2006 and 2013 differ from January 2008 and 2010 as they each experienced a major SSW. The major SSW occurred on 20 January 2006 with temperatures at the winter pole rising from 230 to 260 K (Coy *et al.*, 2009). SSWs are forced by breaking of upward-propagating extratropical Rossby waves. Rossby waves that propagate toward the weak tropical stratospheric winds can break near the subtropics and enhance tropical upwelling. Both November–March 2005–2006 and 2012–2013 present maxima in TTL upwelling (0.8 and 0.9 mm s⁻¹ respectively) about a week after the SSW onset. The comparison of boreal winter 2012–2013 with boreal winter 2005–2006 indicates that years with easterly QBO shear and a major SSW in January correspond to years with anomalous TTL upwelling in November–February with SSW-related peaks during January on top.

In a sense the occurrence of a major SSW in January for 2006 and 2013 is a sign of an increase in subtropical/extratropical wave driving from early boreal winter (November) to the time of the SSW onset in January. To further illustrate this point, Figure 6 displays the distribution of anomalies of EP flux divergence for January 2006, 2008, 2010 and 2013 when TTL upwelling is strongest. The EP flux divergence anomalies are computed with respect to the 4-year mean (2006, 2008, 2010 and 2013) of EP flux divergence for January. During January (Figure 6(a)), the EP-flux vectors split into two branches between ~ 30 and 70°N , with one going equatorward near 30°N and one more vertically near 60°N . Strong EP flux convergence on the order of $7 \text{ m s}^{-1} \text{ day}^{-1}$ is observed near 10 hPa in the NH extratropics (40°–70°N). January 2006 and 2013 present negative anomalies of EP flux divergence $\sim -3 \text{ m s}^{-1} \text{ day}^{-1}$ near 10 hPa in the NH extratropics (40°–70°N). This is coherent with the occurrence of

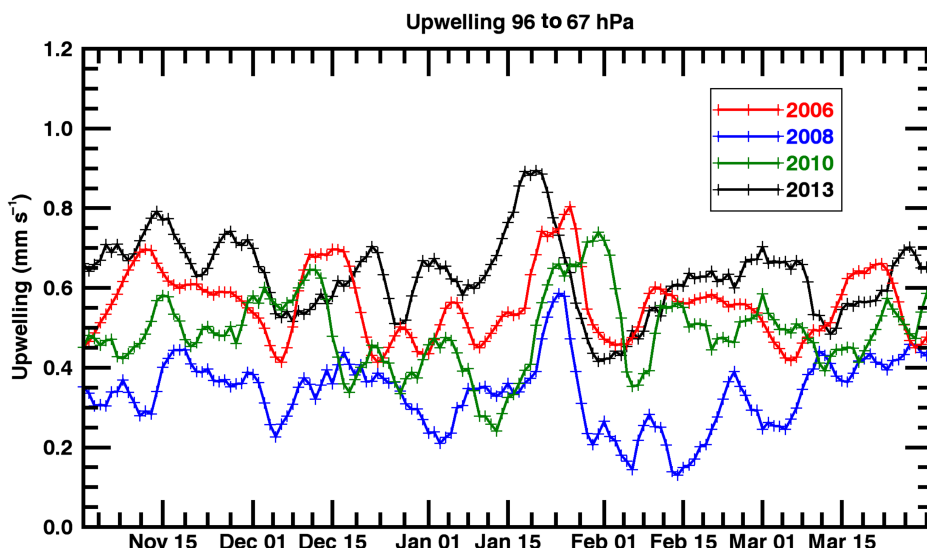


Figure 5. Time series of TTL upwelling (mm s^{-1}) averaged over the Tropics (15°S – 15°N) for boreal winters 2006 (red), 2008 (blue), 2010 (green) and 2013 (black).

a major SSW during these two months. Rossby wave dissipation in this region produces an intensification of the deep branch of the Brewer–Dobson circulation, cooling of the tropical upper stratosphere and warming of the polar stratosphere (Figure 4(a)).

In January 2006 and 2013, anomalous subtropical forcing of $\sim -0.5 \text{ m s}^{-1} \text{ day}^{-1}$ can be seen near 30 hPa near the zero-wind line. Rossby waves generated in the troposphere, which can only propagate through a westerly background flow (Charney and Drazin, 1961), propagate meridionally toward the weak tropical stratospheric winds (marked by the QBO zero-wind line on Figure 5) and dissipate in the subtropics near the QBO zero-wind line. The wave dissipation in the subtropical lower stratosphere could then enhance the shallow branch of the Brewer–Dobson circulation and lead to stronger tropical tropopause cooling. In contrast to 2006 and 2013, January 2008 and 2010 present only weak anomalies in the EP flux divergence in the subtropical lower stratosphere.

A series of recent studies have shown that, in the TTL (particularly below 70 hPa), variability in upwelling and temperature variability is dominated by the shallow branch of the Brewer–Dobson circulation, which is driven by extratropical and tropical wave breaking at lower altitudes near the subtropical tropopause (Grise and Thompson, 2013; Ueyama *et al.*, 2013; Abalos *et al.*, 2014; Ortland and Alexander, 2014). The colder CPT during boreal winters 2005–2006 and 2012–2013 may be attributed to an acceleration of the shallow branch of the Brewer–Dobson circulation by subtropical wave dissipation near the QBO zero-wind line. Bursts of wave activity at the end of December and in the first week of January 2013 in the NH extratropics (Figure 4(d)) lead to Rossby waves propagating meridionally toward the Tropics (Figure 6). Then subtropical wave breaking near the QBO zero-wind line causes enhancement of tropical upwelling in the tropopause region from the end of December to \sim 26 January (Figure 5), thereby contributing to the CPT cooling (Figure 4(b), blue line).

This result is consistent with the enhanced upwelling and cooling observed in the lower stratosphere noted by Gomez-Escalor *et al.* (2014) during an SSW and the easterly shear phase of the QBO. Their composite of EP flux divergence for different years with an SSW and easterly QBO winds (cf. Fig. 5f of Gomez-Escalor *et al.* (2014)) shows stronger subtropical forcing on the order of $1 \text{ m s}^{-1} \text{ day}^{-1}$ near the QBO zero-wind line between 50 and 20 hPa.

3.3. Convection in the Tropics

Figure 7 displays a longitude–time diagram of daily OLR anomalies from 1 November 2012 to 31 March 2013. The daily

OLR anomaly is defined as the difference of OLR value for a given day from its 1980–2013 climatological value. The OLR anomalies were averaged between 15°S and 15°N . Negative OLR anomalies (blue shading) correspond to active convection while positive OLR anomalies (yellow/red shading) correspond to drier conditions. Figure 7 shows that during late December, convection increased over the Indian Ocean with some eastward propagation. This is indicative of developing MJO activity over that region.

Figure 8 shows the MJO phase diagram for 1 December 2012 to 31 January 2013. The axes of the phase diagram correspond to the Real-time Multivariate MJO series 1 (RMM1) and 2 (RMM2). The RMM1 and RMM2 data are from the Australian Bureau of Meteorology and are based on a combined empirical orthogonal function analysis using fields of near-equatorially averaged (15°S – 15°N) 850 and 200 hPa zonal wind and OLR (Wheeler and Hendon, 2004). The MJO phase diagram illustrates the progression of the MJO through different phases, indicating the location of the enhanced phase of the MJO along the Equator around the globe. The MJO cycle, as defined by RMM1 and RMM2, can be split up into eight phases. The distance from the origin is proportional to the MJO strength. When the index is within the centre circle the MJO is considered weak. Counterclockwise motion on the phase diagram is indicative of eastward propagation.

Figure 8 indicates that enhanced convection strengthened over the Indian Ocean while shifting eastward in the last two weeks of December. This is in agreement with the evolution of OLR anomalies between 60 and 100°E shown in Figure 7. The MJO strengthened considerably during the first week of January while propagating across the Maritime Continent; MJO amplitude doubled from 3 to 5 January. The MJO remained active during January and started to weaken and slow down when it reached the International Date Line on 14 January. The MJO remained active into February, although its amplitude was weaker during early February.

Given the description of the MJO by the (RMM1, RMM2) phase space, composites can be formed by averaging the OLR anomalies over days that correspond to each of the eight MJO phases (with MJO amplitude greater than 1). The typical MJO cycle lasts between 30 and 60 days so that each of the eight phases can last between \sim 3–8 days, but there can be considerable variability in these numbers from one MJO event to the next. To compute composites of mean daily OLR anomalies, we follow the method described in Wheeler *et al.* (2008). The OLR anomalies are obtained by subtracting the multiyear climatological OLR mean for boreal winter (December–January–February, DJF). We use the period 2000–2013 to define the multiyear climatological mean for DJF, and the OLR anomalies look very similar if the longer

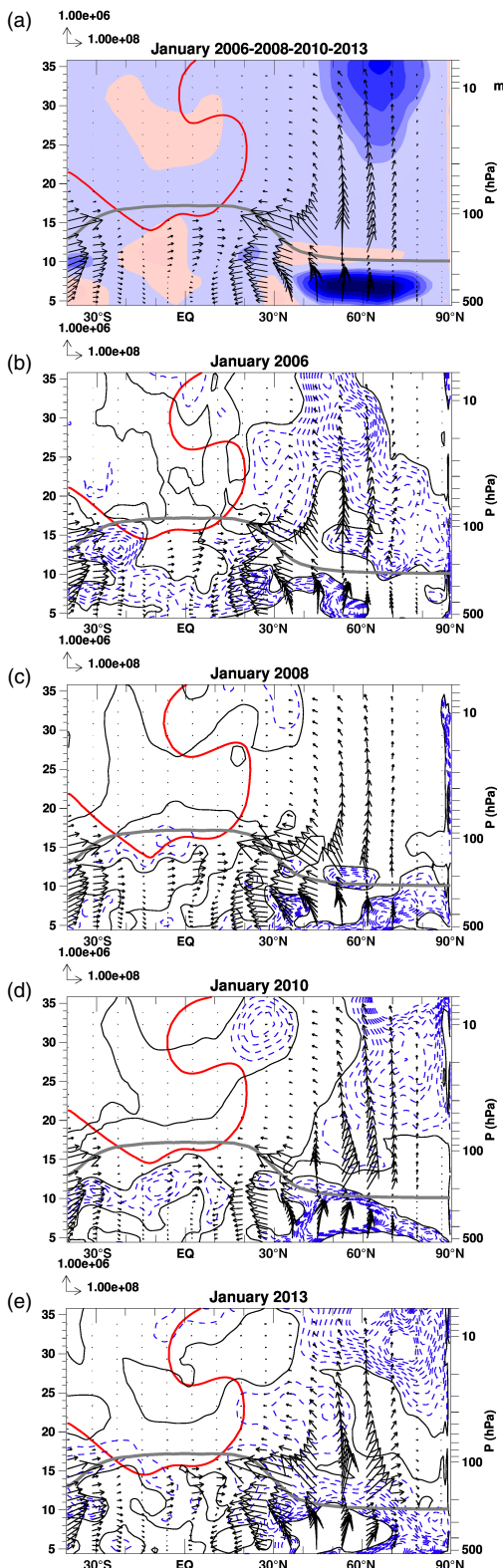


Figure 6. (a) Zonal-mean EP flux vectors and divergence averaged over January 2006/2008/2010/2013. Zonal-mean EP flux vectors and EP flux divergence anomalies from the 4-year mean averaged over (b) January 2006, (c) January 2008, (d) January 2010 and (e) January 2013. A scale factor of 5 is applied for EP flux vectors in the stratosphere. Only negative anomalies of EP flux divergence ($\text{m s}^{-1} \text{ day}^{-1}$) are shown as blue dashed lines. The zero contour is the black solid line. Contours are drawn every $-0.3 \text{ m s}^{-1} \text{ day}^{-1}$. Thick red lines mark the average zero-wind line and thick grey lines mark the average tropopause pressure in all five panels.

time period is used for the climatological mean. Figure 9 presents the composites of OLR anomalies for the MJO events of DJF 2006, 2008, 2010 and 2013 for phases 3–6 of the MJO. As the MJO cycle progresses beyond phase 3, its convective centre shifts eastward from the Indian Ocean (phases 2–3) to the Maritime Continent (phases 4–5) and the western Pacific (phases 6–7). Boreal winters

2006, 2008, 2010 and 2013 experienced similar MJO events with the MJO developing from mid-December to early January and remaining active from most of January–February. The mean MJO amplitudes were 1.8, 1.7, 1.6 and 1.8 for 2006, 2008, 2010 and 2013 respectively. The composites of phase 3 show that the convection is active south of India with suppressed convection near the date-line. By phase 4, enhanced convection can be observed across the eastern Indian Ocean and Indonesia with negative OLR anomalies of $\sim 40 \text{ W m}^{-2}$. The composites of phases 5 and 6 show convection strengthening over the South Pacific Convergence Zone (SPCZ). Convection over the SPCZ was stronger in 2006 and 2008, with OLR anomalies reaching values $\sim 48 \text{ W m}^{-2}$.

Figure 10 shows maps of daily mean CPT temperature anomalies for January 2008, 2010 and 2013. The CPT temperature anomalies are defined as deviations from the climatological DJF mean for 2006–2013. The CPT temperature anomalies were derived after gridding the COSMIC data on a 10° latitude $\times 10^\circ$ longitude grid. We did not use the CHAMP data to produce the map of daily mean CPT temperature anomalies for January 2006 because CHAMP has much sparser data coverage than COSMIC in the Tropics (~ 60 profiles per day between 30°S and 30°N). Both January 2008 and 2013 present negative CPT temperature anomalies over the Maritime Continent and the western Pacific, but January 2013 is much colder than January 2008 and 2010. In January 2013, a minimum of -3.2 K in CPT temperature anomalies is observed over the central Pacific and a secondary minimum of -2.4 K is observed over Africa. The zonally averaged CPT temperature anomalies for the deep Tropics (15°S – 15°N) are -0.34 , -0.2 and -1.52 K for January 2008, 2010 and 2013 respectively.

It has been shown that El Niño–Southern Oscillation (ENSO) can influence CPT temperatures. Zhou *et al.* (2001) showed that the CPT temperature anomalies over the western Pacific are about 0.4 K (-0.4 K) during El Niño (La Niña) events. In boreal winters 2008, 2010 and 2013, the Oceanic Niño Index (ONI) was -1.5 , 1.6 and -0.6 K respectively. The ONI is based on the 3-month running-mean sea-surface temperature (SST) departures from average in the Niño-3.4 region of the equatorial Pacific Ocean (5°N – 5°S , 170 – 120°W). It is considered to be La Niña (El Niño) conditions when the Oceanic Niño Index (ONI) value is less than -0.5 K (greater than 0.5 K). According to the ONI, a La Niña episode began in July–August–September 2007 and ended during April–May–June 2008 (not shown). In 2008, the ONI reached its minimum value of -1.5 K during the 3-month period of DJF. La Niña conditions in DJF 2008 could contribute to the north–south dumbbell of positive CPT anomalies $\sim 0.8 \text{ K}$ over the central Pacific and the cold anomaly over the western Pacific (see Fig. 11 of Zhou *et al.*, 2001). El Niño conditions in January 2010 produce an opposite pattern in CPT temperature anomalies with warm CPT anomalies over the western Pacific and negative CPT anomalies over the central Pacific. However January 2013 corresponds to neutral ENSO conditions and it is unlikely that the negative CPT anomalies over most of the Tropics can be attributed to ENSO.

Virts and Wallace (2014) examined the relationship between MJO-related convection and TTL temperatures, circulation, cirrus and trace gases. They used four years of COSMIC data (2006–2010) to compute composites of COSMIC 100 hPa temperatures for various phases of the MJO. The COSMIC data were first gridded on a 10° latitude $\times 10^\circ$ longitude grid. An 80-day high-pass Lanczos filter was then applied to the time series of COSMIC temperature at each grid box. The filtered temperature time series were regressed onto a linear combination of RMM1 and RMM2 time series corresponding to different phases of the MJO (e.g. RMM1 + RMM2 corresponds to phases 5–6 in the MJO phase space). The 100 hPa ERA-Interim temperature anomalies associated with the MJO are shown in Fig. 3 of Virts and Wallace (2014). Note that they obtained similar patterns and amplitudes by analysing COSMIC CPT temperatures. As the MJO convective envelope propagates eastward from the Indian Ocean to the

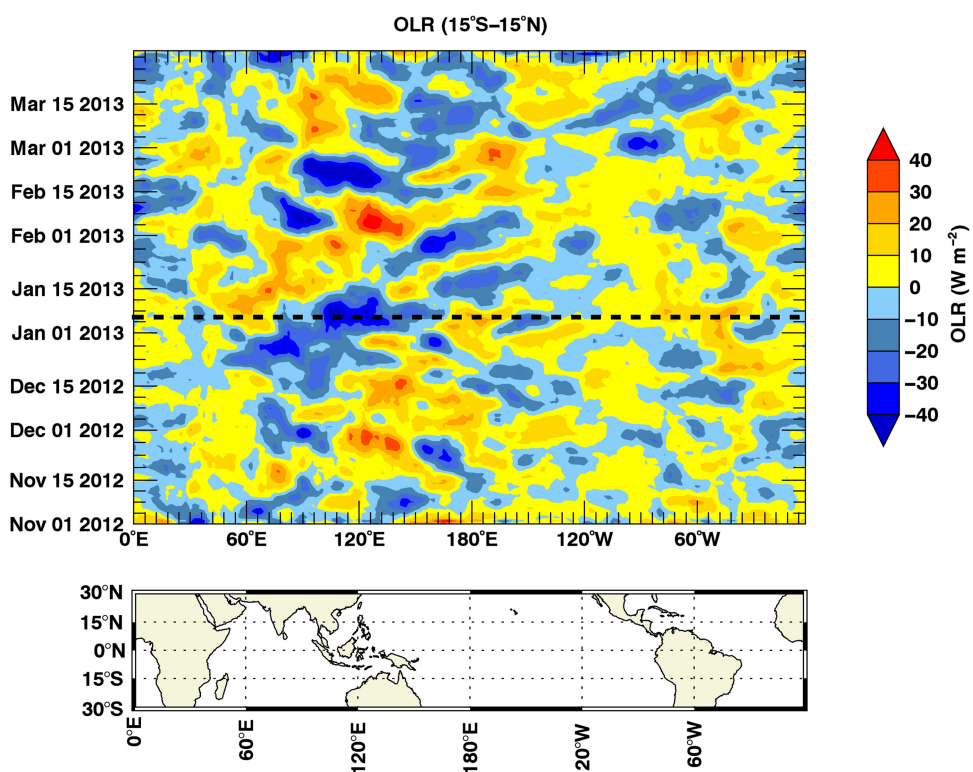


Figure 7. Time–longitude section of OLR anomalies (W m^{-2}) averaged from 15°S to 15°N from 1 November 2012 to 31 March 2013. The dashed black line indicates the SSW onset on 6 January.

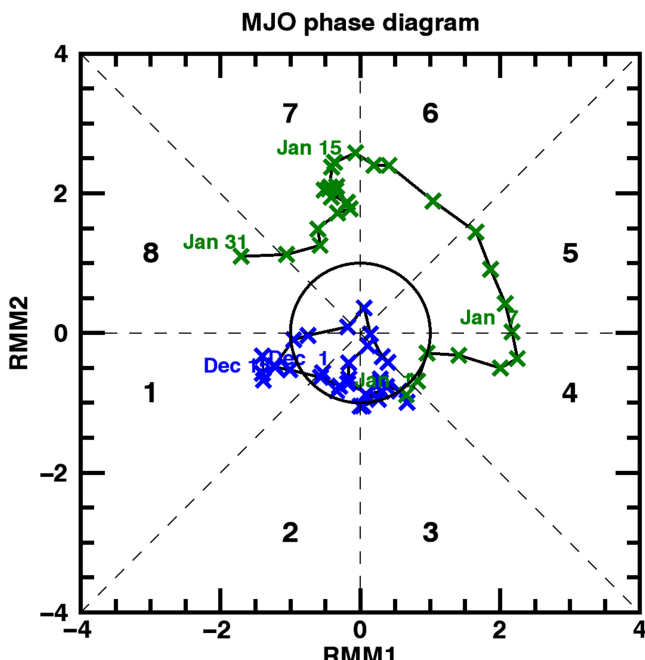


Figure 8. MJO phase space diagram from 1 December 2012 to 31 January 2013. The axes (RMM1 and RMM2) represent daily values of the principal components from the two leading modes. The triangular areas indicate the location of enhanced phase of the MJO. Distance from the origin is proportional to MJO strength. The blue line is for December and the green line is for January. Labelled dots correspond to days of December and January. Also shown are the eight defined phases of the MJO (bold black numbers).

western Pacific (see phases 3–7, Fig. 2 of Virts and Wallace, 2014), a planetary-scale region of anomalously lower temperatures along the Equator can be seen ahead of the enhanced MJO convection and a region of warmer temperatures is observed to the west of the enhanced MJO convection. These patterns correspond to Kelvin and Rossby wave responses to diabatic heating due to the MJO convection over the Equator. The coldest MJO temperature anomalies (-0.8 K) are observed over the Maritime Continent

(Fig. 3b of Virts and Wallace, 2014) during phases 4–5. From phases 5 to 7, a second region of negative COSMIC temperature anomalies of -0.4 K can be seen over South America. La Niña and MJO conditions combined could explain a large fraction of the amplitude of the cold CPT temperature anomalies (-1.5 K) observed over the Maritime Continent/western Pacific during January 2008 (Figure 10). The amplitude of the cold anomaly (-0.5 K) over South America during January 2008 is also coherent with the cold region over that region during phases 5–7 of the MJO. January 2013 experienced neutral ENSO conditions and Figure 9 shows MJO OLR anomalies that have fairly similar amplitudes in January 2008 and January 2013. Hence the MJO convection by itself cannot explain the very cold CPT anomalies observed near 180°E in the western Pacific (-3.2 K) and most of the Tropics during January 2013. This suggests that enhanced extratropical planetary wave and TTL upwelling associated with the January 2013 SSW largely contributed to the cold CPT temperature anomalies observed on Figure 10.

Garfinkel *et al.* (2012) proposed a connection between SSWs and the MJO. They looked at major, midwinter SSWs and phase of the MJO during boreal winters from 1979 to 2011 and found that major SSWs tend to follow certain MJO phases. A month before an SSW the MJO tends to be in phase 2 or 3; phases 4, 6 and 7 are preferred 13–24 days before SSWs and phases 7–8 are preferred 12 days prior to SSWs. They suggested that tropical diabatic heating associated with the MJO excites subtropical planetary waves which then propagate poleward and upward and affect the polar vortex. Figure 8 shows that the MJO remained weak in December 2012, prior to the SSW. Therefore it is difficult to infer whether the MJO contributed to driving the major SSW of January 2013.

4. Summary

In this study, we examined an event during boreal winter 2013 where multiple observations showed extreme negative anomalies in TTL water vapour concentrations. In February 2013, both *in situ* measurements of water vapour from the ATTREX experiment and MLS satellite show dry values ($\sim 2\text{ ppmv}$) in the TTL over

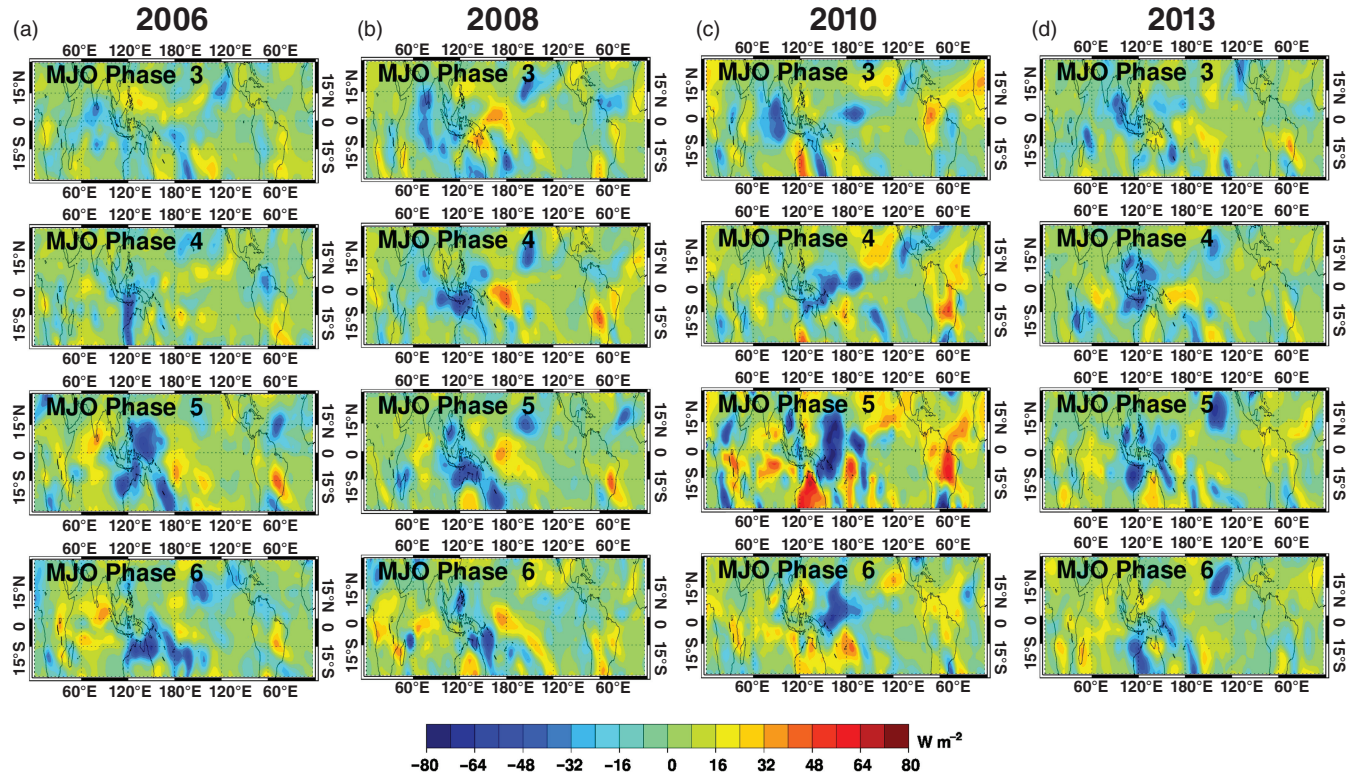


Figure 9. MJO composites of daily mean OLR anomalies for (a) December–January–February (DJF) 2006, (b) DJF 2008, (c) DJF 2010 and (d) DJF 2013.

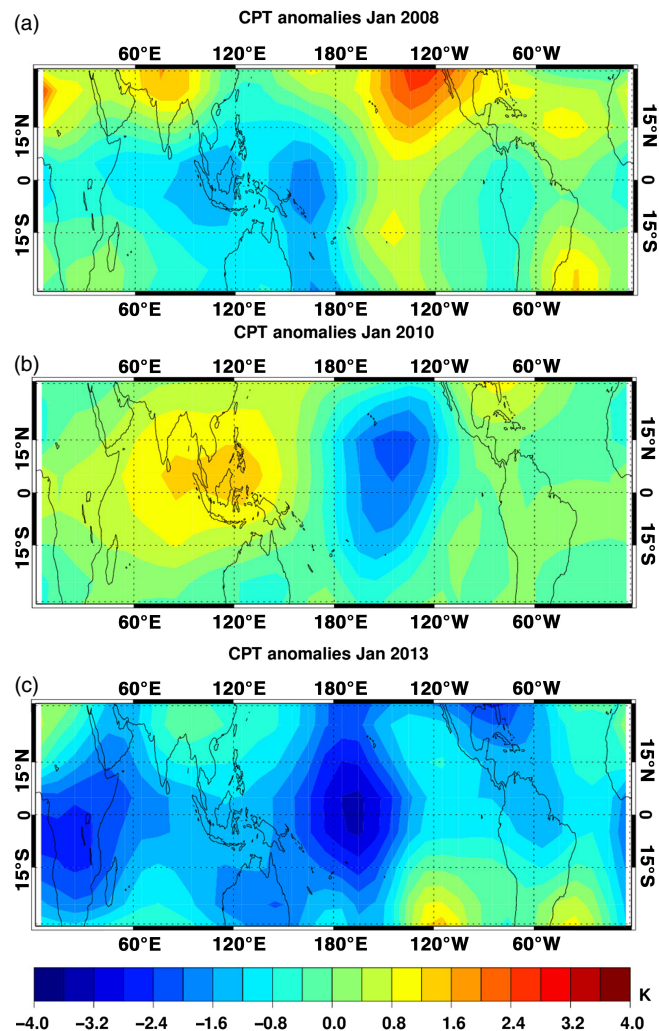


Figure 10. COSMIC CPT temperature anomalies averaged over (a) January 2008, (b) January 2010 and (c) January 2013.

the eastern Pacific. The February 2013 zonally averaged tropical monthly-mean value of MLS water vapour satellite data at 82 hPa (2.3 ppmv) was one of the lowest during the MLS record (2004–2013). The extremely low water vapour concentrations in the TTL were likely due to dehydration of air by horizontal motion through very cold regions observed in the deep Tropics during January 2013. The COSMIC data show that there was a rapid cooling of the tropical CPT starting at the end of December. The tropical CPT temperature decreased by about 2 K within the first 15 days of January and the CPT altitude increased by ~ 400 m. The rapid CPT cooling was likely a consequence of the interactions of a major SSW event in January 2013, the easterly shear phase of the QBO, and the MJO being active over the Maritime Continent/western Pacific during January.

We used ERA-Interim data to estimate TTL upwelling for January 2013 when TTL temperatures were coldest. We compared the TTL upwelling for years that experienced January SSWs and easterly QBO shear (2006 and 2013) to years with easterly QBO shear, without a January SSW (2008 and 2010). January 2006 and 2013 had stronger TTL upwelling and corresponding colder CPT temperatures. For both years, stronger EP flux convergence can be seen near 30 hPa in the subtropics ($20\text{--}30^\circ\text{N}$) near the QBO zero-wind line. The stronger subtropical EP flux convergence near 30 hPa during January 2006 and 2013 would have intensified the tropical upwelling between 100 and 30 hPa, resulting in colder CPT over the Tropics in January and corresponding dry TTL values in February. In addition, boreal winters 2006, 2008, 2010 and 2013 experienced fairly similar MJO events but January 2006 and 2013 presented much colder CPT temperatures. Therefore the MJO convection by itself cannot explain the very cold CPT anomalies observed during January 2013.

The mechanism for dehydration of air entering the stratosphere is not completely understood, but we do know there is a relation with CPT (Fueglistaler *et al.*, 2009), albeit not a perfect correlation when considering trends. We show here a case (winter 2012/2013) with an extremely dry entry value of stratospheric water vapour (one of the lowest on record) where the QBO phase and the existence of a midwinter sudden stratospheric warming appear to have played a role. This is a single case-study; additional modelling and analysis work for other SSW events will be necessary to reduce

the uncertainties, and validate the conclusion regarding how a major SSW can influence TTL cooling.

References

- Abalos M, Randel WJ, Serrano E. 2014. Dynamical forcing of subseasonal variability in the tropical Brewer–Dobson circulation. *J. Atmos. Sci.* **71**: 3439–3453.
- Andrews DG, Holton JR, Leovy CB. 1987. *Middle Atmospheric Dynamics*. Academic Press: San Diego, CA.
- Anthes RA, Ector D, Hunt DC, Kuo Y-H, Rocken C, Schreiner WS, Sokolovskiy SV, Syndergaard S, Wee T-K, Zeng Z, Bernhardt PA, Dymond KF, Chen Y, Liu H, Manning K, Randel WJ, Trenberth KE, Cucurull L, Healy SB, Ho S-P, McCormick C, Meehan TK, Thompson DC, Yen NL. 2008. The COSMIC/FORMOSAT-3 mission: Early results. *Bull. Am. Meteorol. Soc.* **89**: 313–333.
- Birner T, Bönisch H. 2011. Residual circulation trajectories and transit times into the extratropical lowermost stratosphere. *Atmos. Chem. Phys.* **11**: 817–827.
- Brewer AW. 1949. Evidence for a world circulation provided by the measurements of helium and water vapour distribution in the stratosphere. *Q. J. R. Meteorol. Soc.* **75**: 351–363.
- Charney JG, Drazin PG. 1961. Propagation of planetary-scale disturbances from the lower into the upper atmosphere. *J. Geophys. Res.* **66**: 83–109, doi: 10.1029/JZ066i001p00083.
- Coy L, Eckermann SD, Hoppel K. 2009. Planetary wave breaking and tropospheric forcing as seen in the stratospheric sudden warming of 2006. *J. Atmos. Sci.* **66**: 495–507, doi: 10.1175/2008JAS2784.1.
- Dee DP, Uppala SM, Simmons AJ, Berrisford P, Poli P, Kobayashi S, Andrae U, Balmaseda MA, Balsamo G, Bauer P, Bechtold P, Beljaars ACM, van de Berg L, Bidlot J, Bormann N, Delsol C, Dragani R, Fuentes M, Geer AJ, Haimberger L, Healy SB, Hersbach H, Hölm EV, Isaksen L, Källberg P, Köhler M, Matricardi M, McNally AP, Monge-Sanz BM, Morcrette JJ-J, Park B-K, Peubey C, de Rosnay P, Tavolato C, Thépaut J-N, Vitart F. 2011. The ERA-Interim reanalysis: Configuration and performance of the data assimilation system. *Q. J. R. Meteorol. Soc.* **137**: 553–597.
- Dima IM, Wallace JM. 2007. Structure of annual-mean equatorial planetary waves. *J. Atmos. Sci.* **64**: 2862–2880.
- Eguchi N, Kodera K. 2010. Impacts of stratospheric sudden warming event on tropical clouds and moisture fields in the TTL: A case study. *SOLA* **6**: 137–140.
- Eguchi N, Kodera K, Nasuno T. 2015. A global non-hydrostatic model study of a downward coupling through the tropical tropopause layer during a stratospheric sudden warming. *Atmos. Chem. Phys.* **15**: 297–304.
- Evans S, Rosenlof KH, Dudhia J, Hassler B, Davis SM. 2013. The representation of the TTL in a tropical channel version of the WRF model. *J. Geophys. Res. Atmos.* **118**: 2835–2848, doi: 10.1002/jgrd.50288.
- Fueglistaler S, Bonazzola M, Haynes PH, Peter T. 2005. Stratospheric water vapor predicted from the Lagrangian temperature history of air entering the stratosphere in the Tropics. *J. Geophys. Res.* **110**: D08107, doi: 10.1029/2004JD005516.
- Fueglistaler S, Dessler AE, Dunkerton TJ, Folkins I, Fu Q, Mote PW. 2009. Tropical tropopause layer. *Rev. Geophys.* **47**: RG1004, doi: 10.1029/2008RG000267.
- Garfinkel CI, Feldstein SB, Waugh DW, Yoo C, Lee S. 2012. Observed connection between stratospheric sudden warmings and the Madden–Julian Oscillation. *Geophys. Res. Lett.* **39**: L18807, doi: 10.1029/2012GL053144.
- Gettelman A, Birner T. 2007. Insights on tropical tropopause layer processes using global models. *J. Geophys. Res.* **112**: D23104, doi: 10.1029/2007JD008945.
- Gómez-Escalor M, Calvo N, Barriopedro D, Fueglistaler S. 2014. Tropical response to stratospheric sudden warmings and its modulation by the QBO. *J. Geophys. Res. Atmos.* **119**: 7382–7395, doi: 10.1002/2013JD020560.
- Grise KM, Thompson DWJ. 2013. On the signatures of equatorial and extratropical wave forcing in tropical tropopause layer temperatures. *J. Atmos. Sci.* **70**: 1084–1102.
- Holton JR, Tan H-C. 1980. The influence of the equatorial Quasi-Biennial Oscillation on the global circulation at 50 mb. *J. Atmos. Sci.* **37**: 2200–2208.
- Holton JR, Haynes PH, McIntyre ME, Douglass AR, Rood RB, Pfister L. 1995. Stratosphere–troposphere exchange. *Rev. Geophys.* **33**: 403–439.
- Hurst DF, Lambert A, Read WG, Davis SM, Rosenlof KH, Hall EG, Jordan AF, Oltmans SJ. 2014. Validation of Aura Microwave Limb Sounder stratospheric water vapor measurements by the NOAA frost point hygrometer. *J. Geophys. Res. Atmos.* **119**: 1612–1625, doi: 10.1002/2013JD020757.
- Juckes M. 2001. A generalization of the transformed Eulerian–mean meridional circulation. *Q. J. R. Meteorol. Soc.* **127**: 147–160.
- Kodera K. 2006. Influence of stratospheric sudden warming on the equatorial troposphere. *Geophys. Res. Lett.* **33**: L06804, doi: 10.1029/2005GL024510.
- Kodera K, Eguchi N, Lee JN, Kuroda Y, Yukimoto S. 2011. Sudden changes in the tropical stratospheric and tropospheric circulation during January 2009. *J. Meteorol. Soc. Jpn.* **89**: 283–290.
- Kuang Z, Bretherton CS. 2004. Convective influence on the heat balance of the tropical tropopause layer: A cloud-resolving model study. *J. Atmos. Sci.* **61**: 2919–2927.
- Kursinski ER, Hajj GA, Schofield JT, Linfield RP, Hardy KR. 1997. Observing Earth's atmosphere with radio occultation measurements using the Global Positioning System. *J. Geophys. Res.* **102**: 23429–23465, doi: 10.1029/97JD01569.
- Liebmann B, Smith CA. 1996. Description of a complete (interpolated) outgoing longwave radiation dataset. *Bull. Am. Meteorol. Soc.* **77**: 1275–1277.
- Matthew C, Wheeler Harry H, Hendon Sam Cleland, Holger Meinke, Alexis Donald. 2009. Impacts of the Madden–Julian oscillation on Australian rainfall and circulation. *J. Climate* **22**: 1482–1498, doi: http://dx.doi.org/10.1175/2008JCLI2595.1.
- McInturff RM. 1978. 'Stratospheric warmings: Synoptic, dynamic and general-circulation aspects', Technical Report NASA-RP-1017. NASA, Reference Publication: Washington, DC.
- Mastenbrook HJ, Oltmans SJ. 1983. Stratospheric water vapor variability for Washington, DC/Boulder, CO: 1964–1982. *J. Atmos. Sci.* **40**: 2157–2165.
- Matsuno T. 1971. A dynamical model of the stratospheric sudden warming. *J. Atmos. Sci.* **28**: 1479–1494.
- Orland DA, Alexander MJ. 2014. The residual-mean circulation in the tropical tropopause layer driven by tropical waves. *J. Atmos. Sci.* **71**: 1305–1322.
- Plumb RA, Bell RC. 1982. A model of the quasi-biennial oscillation on an equatorial beta-plane. *Q. J. R. Meteorol. Soc.* **108**: 335–352.
- Rosenlof KH. 1995. Seasonal cycle of the residual mean meridional circulation in the stratosphere. *J. Geophys. Res.* **100**: 5173–5191, doi: 10.1029/94JD03122.
- Shimizu A, Tsuda T. 2000. Variations in tropical tropopause observed with radiosondes in Indonesia. *Geophys. Res. Lett.* **27**: 2541–2544, doi: 10.1029/1999GL011269.
- Solomon S, Rosenlof KH, Portmann RW, Daniel J, Davis SM, Sanford T, Plattner G-K. 2010. Contributions of stratospheric water vapor changes to decadal variations in the rate of global warming. *Science* **327**: 1219–1223, doi: 10.1126/science.1182488.
- Thornberry TD, Rollins AW, Gao RS, Watts LA, Ciciora SJ, McLaughlin RJ, Fahey DW. 2014. A two-channel, tunable diode laser-based hygrometer for measurement of water vapor and cirrus cloud ice water content in the upper troposphere and lower stratosphere. *Atmos. Meas. Tech. Discuss.* **7**: 8271–8309, doi: 10.5194/amtd-7-8271-2014.
- Thuburn J, Craig GC. 2000. Stratospheric influence on tropopause height: The radiative constraint. *J. Atmos. Sci.* **57**: 17–28.
- Ueyama R, Gerber EP, Wallace JM, Frierson DMW. 2013. The role of high-latitude waves in the intraseasonal to seasonal variability of tropical upwelling in the Brewer–Dobson circulation. *J. Atmos. Sci.* **70**: 1631–1648.
- Virts KS, Wallace JM. 2014. Observations of temperature, wind, cirrus, and trace gases in the tropical tropopause transition layer during the MJO. *J. Atmos. Sci.* **71**: 1143–1157.
- Wheeler MC, Hendon HH. 2004. An all-season real-time multivariate MJO index: Development of an index for monitoring and prediction. *Mon. Weather Rev.* **132**: 1917–1932.
- Xue Long Zhou, Marvin A. Geller, Ming Hua Zhang. 2001. Tropical cold point tropopause characteristics derived from ECMWF reanalyses and soundings. *J. Climate* **14**: 1823–1838, doi: http://dx.doi.org/10.1175/1520-0442(2001)014<1823:TCPTCD>2.0.CO;2.
- Yoshida K, Yamazaki K. 2011. Tropical cooling in the case of stratospheric sudden warming in January 2009: Focus on the tropical tropopause layer. *Atmos. Chem. Phys.* **11**: 6325–6336.
- Yuan W, Geller MA, Love PT. 2014. ENSO influence on QBO modulations of the tropical tropopause. *Q. J. R. Meteorol. Soc.* **140**: 1670–1676.